

Article

# Design Longitudinal Control System Using Suitable T-Foil Modeling for the Offshore Wind Power Operation and Maintenance Vessel with Severe Sea States

Jia Yuan <sup>1</sup>, Zhen Liu <sup>1,\*</sup>, Hua Geng <sup>1</sup>, Songtao Zhang <sup>2,\*</sup>, Lihua Liang <sup>2</sup> and Peng Zhao <sup>3</sup>

- <sup>1</sup> School of Information and Electrical Engineering, Hebei University of Engineering, Handan 056038, China; yuanjia@hebeu.edu.cn (J.Y.); huahua27102710@163.com (H.G.)
- <sup>2</sup> College of Intelligent System Science and Engineering, Harbin Engineering University, Harbin 150001, China; liang\_hrbjyq@126.com
- <sup>3</sup> Department of Transportation and Vehicle Engineering, Tangshan University, Tangshan 063000, China; heuzyyby@163.com
- \* Correspondence: liuzhen@hebeu.edu.cn (Z.L.); hrbzst@126.com (S.Z.); Tel.: +86-15832040790 (Z.L.); +86-13946032279 (S.Z.)

**Abstract:** In order to reduce the offshore wind power operation and maintenance vessel motion induced by severe sea states, a suitable stabilizer with the ship based on linear quadratic regulator strategy is proposed in this paper. First of all, the dynamics of the ship motion model are established to study the longitudinal control system. The six degrees of freedom nonlinear motion model and nonlinear coupled longitudinal motion (heave and pitch) model are described in detail in this paper. Secondly, this work presents matching suitability between the T-foil and the operation and maintenance vessel. Therefore, the most suitable installation position and the optimum strut's height of T-foil are determined by meshing the ship hull model, setting the water channel, and a series of corresponding computer fluid dynamic simulation. Following that, the linear quadratic regulator controller is studied with active longitudinal control system based on the suitable T-foil. Furthermore, a longitudinal control system is built, including free vessel module and the suitable T-foil stabilizer-based proposed controller module. Finally, the simulation results indicate that the designed T-foil and the longitudinal control system are feasible and effective to ensure the heave and pitch motion reduction based on the proposed controller.

**Keywords:** longitudinal control system; suitable T-foil modeling; heave reduction; pitch reduction; severe sea states



**Citation:** Yuan, J.; Liu, Z.; Geng, H.; Zhang, S.; Liang, L.; Zhao, P. Design Longitudinal Control System Using Suitable T-Foil Modeling for the Offshore Wind Power Operation and Maintenance Vessel with Severe Sea States. *J. Mar. Sci. Eng.* **2023**, *11*, 2182. <https://doi.org/10.3390/jmse11112182>

Academic Editor: Kostas Belibassakis

Received: 17 October 2023  
Revised: 10 November 2023  
Accepted: 14 November 2023  
Published: 16 November 2023



**Copyright:** © 2023 by the authors. Licensee MDPI, Basel, Switzerland. This article is an open access article distributed under the terms and conditions of the Creative Commons Attribution (CC BY) license (<https://creativecommons.org/licenses/by/4.0/>).

## 1. Introduction

Due to the massive consumption of fossil fuels, global environmental issues cannot be ignored, and seeking the development and utilization of renewable energy has become a research focus. Wind power has become one of the ideal renewable energy options for achieving emission reduction goals. Therefore, in recent years, offshore wind power has played an important role in China's national energy strategy [1,2].

The offshore wind power service business demands its maintenance personnel to perform quickly and effectively, yet the intricate marine environment raises the bar for offshore wind power operation and maintenance (O&M) boats' seakeeping standards. Establishing a suitable hydrofoil stabilizer is a challenging problem due to its characteristics as a catamaran. Therefore, designing the matching control device that effectively reduces the motion of ships due to different wave environments is paramount. During the last decades, the bilge keels, anti-rolling tanks, fin stabilizers, and rudder-roll reductions are widely used in ship stabilizing. The integrated control of rudder and fin stabilizers were used for the reduction of the roll motion based on modern control strategies [3]. Jin et al. investigated how the rudder fin joint control system affected the performance of the ship's

sailing by developing a reliable  $H_\infty$ -type state feedback model predictive control [4]. Ren et al. established a ship motion control system using the time-scale decomposition approach, implementing rudder roll reduction, based on a four degrees of freedom (4 DOF) maneuvering motion model (surge, sway, roll, and yaw) [5]. Lee et al. created a ship motion system based on a traditional PID control method, regulating the rudder angle and propeller rotation speed to estimate ship performance accurately and guarantee effective ship operation [6]. Moreover, the new anti-rolling devices have also emerged in recent years. Li et al. carried out numerical models and experiments on the hydrodynamic moments and forces at zero velocity from the roll amplitude, flapping frequency, and aspect ratio perspectives of the flapping fins. The efficiency of flapping fins as actuators at zero velocity was confirmed, and the empirical formulae for estimating the forces and moments were obtained [7]. Song et al. conducted experiments on the proposed zero/low speed fin stabilizer at various speeds and hydrofoil profile parameters to obtain the optimal hydrofoil profile for effectively controlling ship roll [8]. A new anti-rolling equipment called the Magnus stabilizer was obtained based on the Magnus effect by analyzing the aspect ratios and lift/drag hydrodynamic characteristics [9,10].

A large focus has recently been placed on the catamarans. The transverse stability of a catamaran is higher than a monohull ship because the width of the vessel is much wider than that of a mono-hull ship. A catamaran's thin and long demi-hulls can aid in decreasing wave resistance while maintaining fast speeds [11,12]. However, the heave and pitch motion are very obvious because of the above characteristics of the catamarans at high speeds and severe sea states. The heave and pitch motion can threaten the safety of passengers, crew, and cargo. More seriously, the equipment on the ship will appear to have momentary failure. Based on this, it is essential to install control stabilizers on the catamarans [13]. Zong et al. conducted towing tank experiments using three distinct ship models, including a bare hull, a hull with a non-controlled T-foil, and a hull with an actively controlled T-foil. We confirmed that the T-foil is an efficient appendage for improving trimaran seakeeping performance by comparing different testing situations [14]. The work of Zhu's team used the T-foil or trim tab to reduce the motions of fast catamaran and trimaran, and the significant anti-vertical motion results indicated the importance of installing devices [15–17]. Lau et al. restricted the vertical motion of the vessel on a wave piercing catamaran by installing a T-foil and stern tabs, lowering motion sickness incidence (MSI) and enhancing passenger comfort [18]. Based on a hybrid control method, Jiang et al. presented a T-foil that can greatly improve the seakeeping performance of a high-speed trimaran [19].

Although different types of control equipment can be installed on the catamaran to reduce the ship motion, the general conventional control device can not achieve the ideal stabilizing efficiency, or can even have no effect in actual navigation when the ship is in complex and changeable sea conditions. Thus, designing a stabilizer that is suitable for specific ship types is very important and meaningful. According to the different degrees of the ship motion, the stabilizer constrained by the hull is designed to obtain the best matching parameters, in order to achieve the best stabilization effect. The case studies in [20] elaborated on the control of longitudinal motion of high-speed mono-hull ships, with a focus on analyzing the matching between T-foil and the hull, as well as the stabilization effect on the hull. Finally, an optimized model of T-foil was obtained. Liang et al. proposed a suitable T-foil by analyzing the optimum installation location and the strut's height. Results show that the fitted T-foil is at an advantage over the heave and pitch reduction, and the seakeeping of the wave-piercing catamaran is improved effectively [21].

However, a fixed or suitable stabilizer can suppress ship motion within a certain range, and these control devices cannot provide timely feedback in complex marine environments. The ship ride control system (RCS) has been offered as a solution to the fixed hydrofoil constraint, and several solutions have been investigated by researchers. Davis et al. investigated an 86 m high-speed catamaran with active T-foils and stern flaps. They compared movements estimated through a rapid, fixed-frame, time-based domain strip hypothesis

that took the T-foil and two flaps into account. The acceleration levels at various locations were computed [22]. A data-based linear quadratic Gaussian (LQG) controller for reference tracking was established using the Markov parameters, and a detailed study was conducted on tensegrity morphing airfoils [23]. The active T-foil and two flaps were used for catamaran- or trimaran-based Kalman filter methods. The feasibility and effectiveness of the devices installed on multi-hull ship were proved by the results from their simulations [24,25]. Liang et al. demonstrated a nonlinear feedback system for controlling the fin stabilizer. The controller and feedback error decoration were used to create a type of nonlinear feedback control. The results showed that the performance of controller was not affected and the energy was saved in rough sea [26]. The reference [27] investigated a robust fuzzy controller design problem for discredibly and perturbed nonlinear ship fin stabilizing system. To demonstrate the feasibility and usefulness of the suggested robust fuzzy control approach, a simulation for managing a discrete-time nonlinear ship fin stabilizing system was presented. Zhang et al. suggested a model predictive control strategy for anti-pitching the multi-hull without violating the control input limitations, and simulations and tests demonstrated the control efficacy [28]. Cao et al. suggested a succinct and robust controller for the particular vessels that has a strong pitching reduction impact, anti-interference ability, and energy-saving effect. The controller's efficacy was validated by theoretical analysis and simulated trials under varied scenarios [29].

According to a study of previous studies, most controllers are based on discrete devices that are not confined by the hull. The actual situation is that when the control device is installed on the hull, its lift characteristics will be affected by the hull. Our proposition takes into consideration both the installation position and the strut's height of T-foil [30]. Therefore, the longitudinal control system for suitable T-foil models constrained by the hull is proposed in this paper. The controller's efficiency is validated by theoretical research and simulated studies in extreme sea situations. The main contributions of this study are as follows:

- The two degrees of freedom (2 DOF) motion (heave and pitch) model discussed in this paper contains coupled motion model, which is more general and more complex than the systems with one degree of freedom motion. The existence of coupled longitudinal motion makes the design process of ride control system more complicated;
- The most suitable installation position and the optimum strut's height of T-foil are determined by meshing the ship hull model, setting the water channel, and a series of corresponding computer fluid dynamic (CFD) simulations at different high sea state numbers (SSN) and speeds;
- The attitude control system for ship multiple degrees of freedom (M DOF)-coupled motion is established, which increases the complexity of system modeling and analysis due to the transformation of the system model from a bare hull model to a model with control devices. The proposed control strategy in this paper effectively suppresses the ship's heave and pitch motion.

The remainder of the study is organized as follows. In Section 2, the mathematical models of six degrees of freedom (6 DOF) for ships and 2 DOF motion for the offshore wind power O&M vessel are described, in which disturbing and control forces and moments are elaborated. Section 3 details the matchability simulation of T-foil for the O&M vessel using the CFD software. Section 4 presents the linear quadratic regulator (LQR) strategy for the offshore wind power O&M vessel with the T-foil stabilizer and the longitudinal control system is built. Moreover, the simulation results demonstrate the efficacy of the suggested controller. In Section 5, some results in various sea conditions and speeds are provided to demonstrate the practicality of the suggested control strategy. The concluding remarks are provided in Section 6.

## 2. Dynamics of Ship Motion

### 2.1. Six Degrees of Freedom Model

Based on Newton’s laws, the studies of marine vehicles’ dynamics are divided into two parts: kinematics, which only treats geometric aspects of motion, and kinetics, which are also divided into two parts: rigid-body dynamics, which consist of vehicle inertia matrix, and mechanics, which are the analyses of the forces and moments causing motion [31].

Figure 1 shows a diagram of a ship coordinate system based on the notations of above picture. The following vectors can describe the general motion of a ship in 6 DOF:

$$\begin{aligned} \eta &= [\eta_1^T, \eta_2^T]^T, \eta_1 = [x, y, z]^T, \eta_2 = [\phi, \theta, \psi]^T \\ v &= [v_1^T, v_2^T]^T, v_1 = [u, v, w]^T, v_2 = [p, q, r]^T \\ \tau &= [\tau_1^T, \tau_2^T]^T, \tau_1 = [X, Y, Z]^T, \tau_2 = [K, M, N]^T \end{aligned} \tag{1}$$

where a ship’s motion descriptions are surge, sway, heave, roll, pitch, and yaw, which is a ship’s 6 DOF motion.  $\eta_1 = [x, y, z]^T$  denotes the displacement of a ship in the  $x, y,$  and  $z$  directions, respectively,  $\eta_2 = [\phi, \theta, \psi]^T$  denotes the rotation angle around the  $x, y,$  and  $z$  axes, respectively,  $v_1 = [u, v, w]^T$  denotes the translational velocity in the  $x, y,$  and  $z$  directions, respectively,  $v_2 = [p, q, r]^T$  denotes the rotational velocity around the  $x, y,$  and  $z$  axes, respectively, and  $\tau_1 = [X, Y, Z]^T$  and  $\tau_2 = [K, M, N]^T$  denote the external force and moment [32].

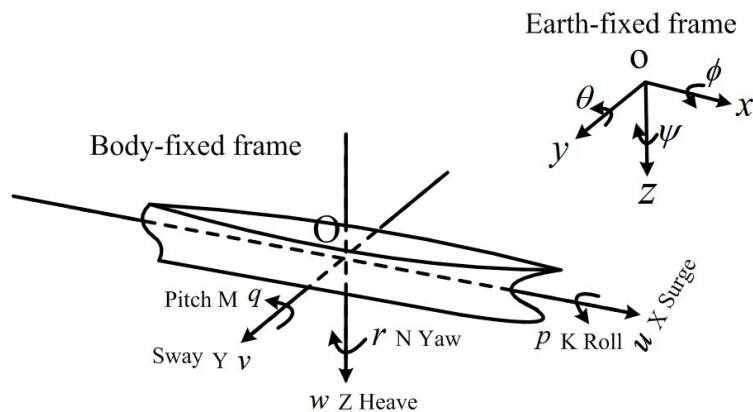


Figure 1. Body-fixed and earth-fixed frame of a ship.

By using the basic principles of dynamics, the general model structure [31] can be conveniently expressed as:

$$M\dot{v} + D(v)v + g(\eta) = \tau_{waves} + \tau_{control} \tag{2}$$

where  $M$  represents the state of inertia matrix and  $D(v)$  represents the fluid damping matrix, which includes potential damping, friction between layers, wave slide damping, and vortex-related damping,  $g(\eta)$  is the gravitational force and moment vector,  $\tau_{waves}$  is the wave interference force and moment vector, and  $\tau_{control}$  is the force and moment vector of control device. When highlighted,  $\dot{\eta} = J(\eta)v, J(\eta)$  is the coordinate transform that connects the translational and rotational velocities of body-fixed and earth-fixed frames,  $J_1(\eta_2)$  represents a transformation matrix connected to the Euler angle, and  $J_2(\eta_2)$  represents a transformation matrix connected to the angular velocity transformation. The expressions of  $J(\eta), J_1(\eta_2),$  and  $J_2(\eta_2)$  are as follows:

$$J(\eta) = \begin{bmatrix} J_1(\eta_2) & 0_{3 \times 3} \\ 0_{3 \times 3} & J_2(\eta_2) \end{bmatrix},$$

$$J_1(\eta_2) = \begin{bmatrix} \cos \theta \cos \psi & \sin \phi \sin \theta \cos \psi - \cos \phi \sin \psi & \cos \phi \cos \psi \sin \theta + \sin \phi \sin \psi \\ \cos \theta \sin \psi & \sin \theta \sin \theta \sin \psi + \cos \theta \cos \psi & \cos \phi \sin \theta \sin \psi - \sin \phi \cos \psi \\ -\sin \theta & \sin \phi \cos \theta & \cos \phi \cos \theta \end{bmatrix},$$

$$J_2(\eta_2) = \begin{bmatrix} 1 & \sin \phi \tan \theta & \cos \phi \tan \theta \\ 0 & \cos \phi & -\sin \phi \\ 0 & \frac{\sin \phi}{\cos \theta} & \frac{\cos \phi}{\cos \theta} \end{bmatrix}.$$

### 2.2. Coupled Equations of Heave and Pitch Motion

Due to the complex and changeable wave disturbances, it is very difficult to solve the hydrodynamic coefficients of the 6 DOF model. In this paper, according to the characteristics of the O&M vessel, motion in surge, sway, roll, and yaw can often be neglected in comparison with the vertical motion, when the ship is traveling at great speeds in head seas [33]. According to the 6 DOF motion model (2), when the origin of the body-fixed frame is located at the center of gravity (CG), the axis of the body-fixed frame is selected on the ship’s inertia spindle, and the smaller hydrodynamic parameters and higher order elements are neglected. The nonlinear coupled equations in 2 DOF based on T-foil reduction model are described as follows [34,35]:

$$\begin{aligned} (m - Z_{\dot{w}})\dot{w} - Z_w w - Z_{w|w}|w|w| - Z_{\dot{q}}\dot{q} - Z_q q \\ - Z_{q|q}|q|q| + mg \cos \phi \cos \theta = Z_{waves} + Z_{T-foil} \\ (I_{yy} - M_{\dot{q}})\dot{q} - M_q q - M_{q|q}|q|q| - M_{\dot{w}}\dot{w} - M_w w \\ - M_{w|w}|w|w| - \rho g \nabla \overline{GM}_L = M_{waves} + M_{T-foil} \end{aligned} \tag{3}$$

where  $Z$  and  $M$  denote forces in the  $Z$  direction and moments with relation to the  $Y$  axis, respectively,  $m$  is the ship mass,  $I_{yy}$  is the inertia about the  $Y$  axis,  $g$  is the acceleration of gravity,  $\rho$  is the water density,  $\nabla$  is the displaced volume of the ship,  $\overline{GM}_L$  is the longitudinal metacentric height, and  $Z_{\dot{w}}$ ,  $Z_w$ ,  $\dots$ , and  $M_{w|w|}$  are the coefficients of the ship’s fluid dynamics and are defined as follows:  $Z_{\dot{w}} = \frac{dZ}{d\dot{w}}$ ,  $Z_w = \frac{dZ}{dw}$ ,  $\dots$ , and  $M_{w|w|} = \frac{dM}{d|w|w|}$  where the terms associated with movements or angles are the hydrodynamic restorative coefficients, the terms associated with speeds are the dynamical damping coefficients, and the ones associated with accelerated velocities are the fluid inertia coefficients. A ship’s hydrodynamic characteristics are sophisticated and change depending on sea state, speed, and so on. As a result, they may be acquired using the formula estimation technique, the computer simulation approach, and the towing tank test methodology.  $Z_{waves}$  and  $M_{waves}$  are the disturbing forces and moments, respectively, caused by wave disturbances, and  $Z_{T-foil}$  and  $M_{T-foil}$  are the control forces and moment,  $m$  respectively, provided by the anti-heaving and pitching stabilizer T-foil.

### 2.3. Wave-Induced Forces and Moments

Waves are incredibly complicated in actuality, and they are the product of irregular random waves. Under the premise of linear theory, complex sea states formed by irregular waves are supplied by adding a huge number of essentially autonomous routine contributions with stages of randomness [36].

Power spectral density (PSD), often known as the wave spectrum, is widely used to define sea conditions. The following expression is used in this research to model fully formed oceans with limitless depth, no swell, and unlimited fetch [37].

$$S(\omega) = \frac{8.1 \times 10^{-3} g^2}{\omega^5} \exp\left(\frac{-3.11}{\omega^4 h_{1/3}^2}\right) \tag{4}$$

where  $g$  is still the gravitational acceleration,  $\omega$  is the wave frequency, and  $h_{1/3}$  is the significant wave height, and it is defined as the average of one-third of the greatest wave amplitude measurements.

The constant wave amplitude of each regular wave component  $\zeta_i$  and the resultant wave  $\zeta(t)$  are calculated by:

$$\zeta_i = \sqrt{2S(\omega_i)\Delta\omega} \tag{5}$$

and

$$\zeta(t) = \sum_{i=1}^n \zeta_i \cos(\omega_i t + \varphi_i) \tag{6}$$

where the subscript  $i$  denotes the  $i$ th regular wave,  $\Delta\omega$  denotes the wave frequency spacing,  $\varphi$  denotes the random phase angle, and it is chosen as a random variable with an average distribution on the interval  $[0, 2\pi]$ .

The disruptive forces  $Z_{waves}$  and moments  $M_{waves}$  in this study are formed using 91 regular parts of waves. They are explained as follows:

$$Z_{waves}(t) = \sum_{i=1}^{91} Z_i \cos(\omega_i t + \varphi_i) \tag{7}$$

$$M_{waves}(t) = \sum_{i=1}^{91} M_i \cos(\omega_i t + \varphi_i)$$

where  $Z_i$  and  $M_i$  are the heave forces and pitch moments produced by the  $i$ th wavelet  $\zeta_i$  disturbance to the hull, respectively.

#### 2.4. T-Foil Lift

An anti-heaving and pitching stabilizer, T-foil, is installed in the bow and it is used to control the longitudinal motion of the O&M vessel. The T-foil is a typical lift hydrofoil. One of the most important characteristics of lift hydrofoil is the pressure difference between upper and lower surfaces of hydrofoil. This difference is produced by changing the attack angle of the hydrofoil. The force analyses are shown in Figure 2.

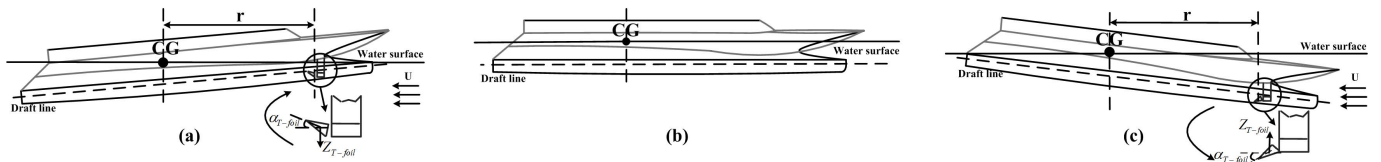


**Figure 2.** The force analyses of T-foil. (a) Lift bow state. (b) Balance state. (c) Submerged bow state.

According to Section 2.2, when the O&M vessel sails at high speeds in head seas, heave and pitch motion are obviously violent. As can be seen from Figure 2, when the ship is in the lift bow state (see Figure 2a), the T-foil located in the bow should provide a downward force to restore the balance of the ship (see Figure 2b). At this point, the attack angle of T-foil needs to be swung from bottom to top to provide the downward force. On the contrary, when the ship is in the submerged bow state (see Figure 2c), the directions of the T-foil’s lift and flap swinging are all in opposition to the above conclusion.

Following that, the control forces  $Z_{T-foil}$  and moments  $M_{T-foil}$  can be expressed as:

$$Z_{T-foil} = \frac{1}{2} \rho A U^2 C_L(\alpha_{T-foil}) \tag{8}$$

$$M_{T-foil} = Z_{T-foil} \cdot r$$

where  $\rho$  is the liquid density,  $A$  is the T-foil’s area,  $U$  is the ship’s speed,  $r$  is the distance between the pressure center of the T-foil and the CG of the ship,  $\alpha_{T-foil}$  is the attack angle of T-foil’s flap, and it can rotate in  $-15^\circ-15^\circ$  with respect to the horizontal, and  $C_L(\alpha_{T-foil})$  is the lift coefficient and it can be obtained by CFD simulation software when the T-foil is in different attack angles.

However, there is a mutual constraint between the T-foil and the hull, so the location and the strut's height of T-foil will be considered as the factors affecting the lift coefficient. Therefore, it will analyze the matchability of T-foil for the O&M vessel from the optimization design of T-foil's location and its strut's height in the next section.

### 3. Matchability Analysis of T-Foil for the O&M Vessel

#### 3.1. CFD Simulation of the O&M Vessel

The offshore wind power O&M vessel is more conducive to navigate at high speeds and reduce the rolling motion, as the ship has two thin and long demi-hulls and a good length and width ratio, and its bow is sharpened (see Figure 3). Based on the three main principles of similarity (geometric similarity, kinematic similarity, and dynamic similarity) [38,39], the original computer simulation hull model will be reduced at a certain scale. This is all for the simulation time-saving and simulation efficiency-improving. The parameters of the original vessel model and its reduced model are listed in Table 1.

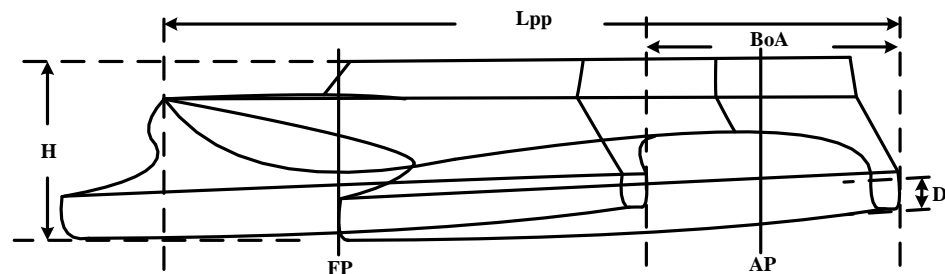


Figure 3. A diagram of the O&M vessel.

Table 1. Parameters of the O&M vessel.

Parameters	Sign	Original Model	Reduced Model	Unit
Length	$L_{pp}$	90.33	10.04	m
Beam overall	$BoA$	25.96	2.88	m
Height	$H$	13.16	1.46	m
Designed draft	$D$	2.60	0.29	m
Displacement	$\nabla$	734.54	1.01	ton

It is necessary to build a precise ship mesh model for the ship simulation. Figure 4 shows the grids of the reduced the O&M vessel model. There are more than one hundred thousand grid units, including triangular and quadrilateral mesh shapes. The deformation degree of the grid model is a crucial parameter in the simulation model. If it is reduced, although the calculation accuracy is improved, it is a great test of computer performance. If it is increased, it saves time and reduces accuracy. Therefore, it needs to be repeatedly verified through trial and error methods to ultimately determine the grid deformation degree of the ship as 0.05.



Figure 4. Mesh model of the O&M vessel.

The mesh model needs to be put in a fluid domain to simulate. Figure 5 shows the parameter settings for the entire fluid domain. In order to determine the accuracy of the simulation data, the dimension design principle of the fluid domain is as follows:

- The length of a fluid domain is about eight times the simulation model's length;
- The height is about eleven times the model's height;

- The width is about three times the model's width.

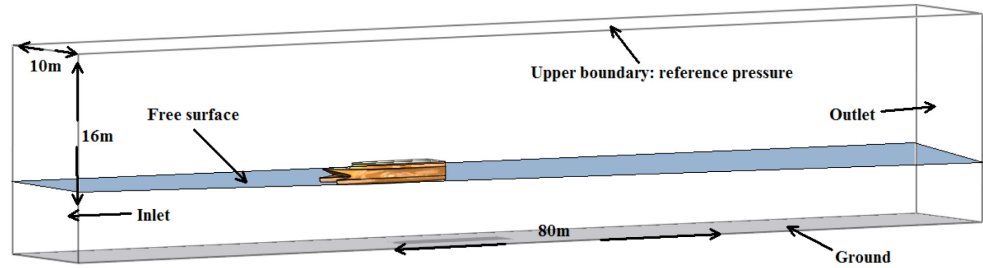


Figure 5. Parameter settings of fluid domain.

Therefore, the dimensions of the reduced O&M vessel model's fluid domain are  $80\text{ m} \times 16\text{ m} \times 10\text{ m}$ . As seen in Figure 5, the flow velocity is set at the inlet surface (the negative direction of  $X$ ), and the positive direction of  $X$  is the outlet surface, the upper boundary (the positive direction of  $Y$ ) is reference pressure, the wall condition is used for the ground surface (the negative direction of  $Y$ ), and the final two sidewalls (the positive and negative direction of  $Z$ ) apply the periodic boundary condition.

When the wave heights increase with the increase of sea states, as shown in Figure 6, the wave crest positions are consistent because of the same speeds. Relatively, the wave heights are consistent when the wave crest positions move faster with the increase of the ship speeds, as shown in Figure 7.

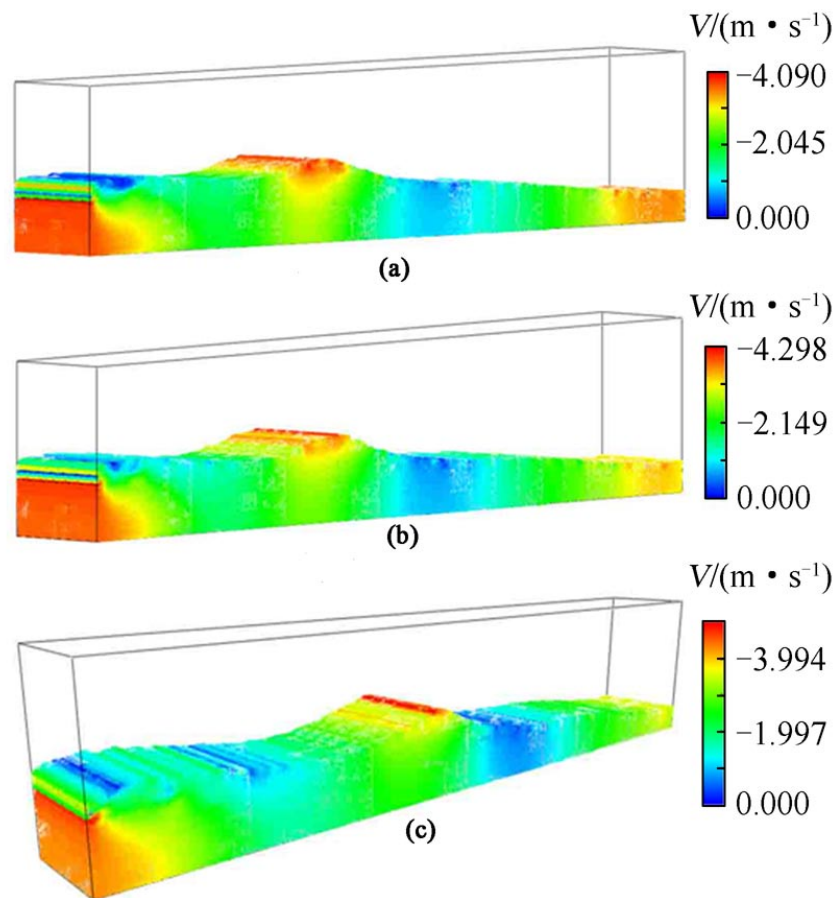
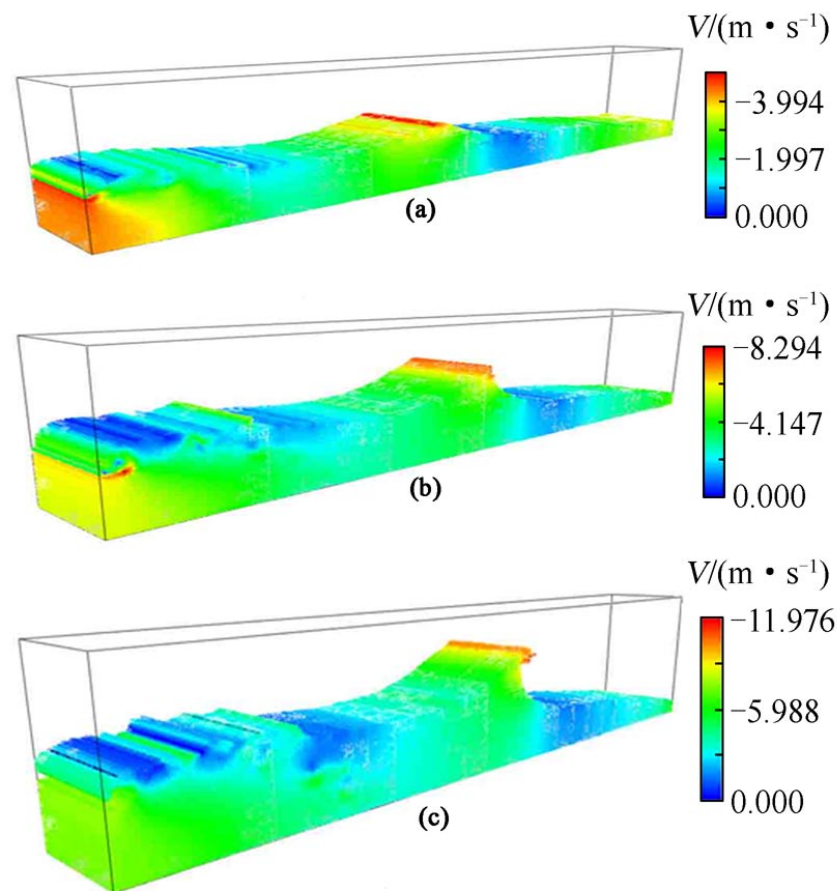


Figure 6. Wave contour of free surface for different sea states ( $t = 4.6\text{ s}$ ). (a) SSN4. (b) SSN5. (c) SSN6.



**Figure 7.** Wave contour of free surface for different speeds ( $t = 4.6$  s). (a) 20 kts. (b) 30 kts. (c) 40 kts.

### 3.2. Optimization Analysis of T-Foil's Location and Strut's Height

According to Section 2.4, when the suitable T-foil for the offshore wind power O&M vessel from the optimization design of T-foil's location and its strut's height is found, the optimal lift coefficient of T-foil will be obtained. Based on CFD simulation, the T-foil's location can be preliminarily judged according to the vessel's attitudes and its wetted area in the following figures [21].

Figures 8 and 9 show the longitudinal attitudes of the O&M vessel in one motion period at different sea conditions and speeds. It is evident that with the rise of the sea state, there is a small upward trend for the ship's heave and pitch motion. However, with the increase of the speed, the heave and pitch motion of the ship fluctuate greatly. Therefore, the change of the speed has a greater influence on the ship motion. Furthermore, with the increase of the sea state and speed, the vertical motion becomes more and more obvious.

Illuminated by [40], the simulation results of different positions of a ship hull show that the foil positioned at the bow is by far the most effective in reducing the longitudinal motion of the vessel. According to Figures 10 and 11, the lifting bow covers 10–44% of the ship length in different sea states and speeds. Therefore, the preliminary judgment of the T-foil's location is obtained and the T-foil should be installed in the distances of 5 m–35 m from the forward perpendicular (FP) of the ship, which is consistent with the above-mentioned literature. Moreover, the final installation position of the T-foil depends on the lift coefficient simulation at a certain location. Figure 12 shows the different locations of T-foil and they are simulated by CFD software at intervals of 5 m (see Figure 13).

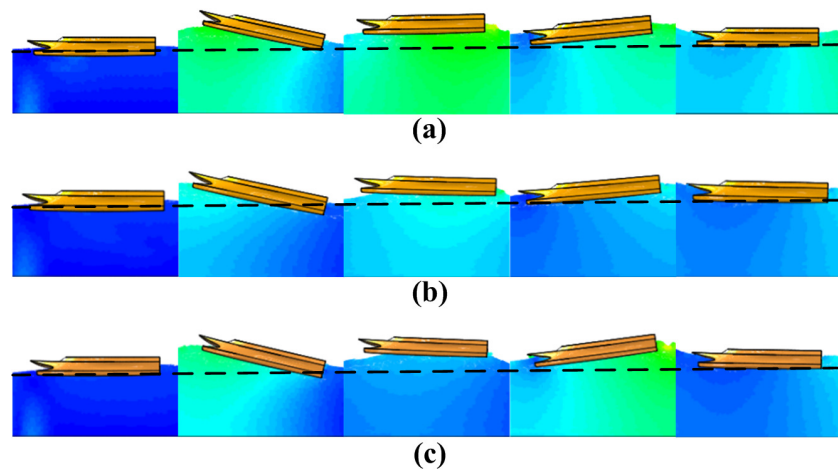


Figure 8. The O&M vessel motion at different sea states. (a) SSN4. (b) SSN5. (c) SSN6.

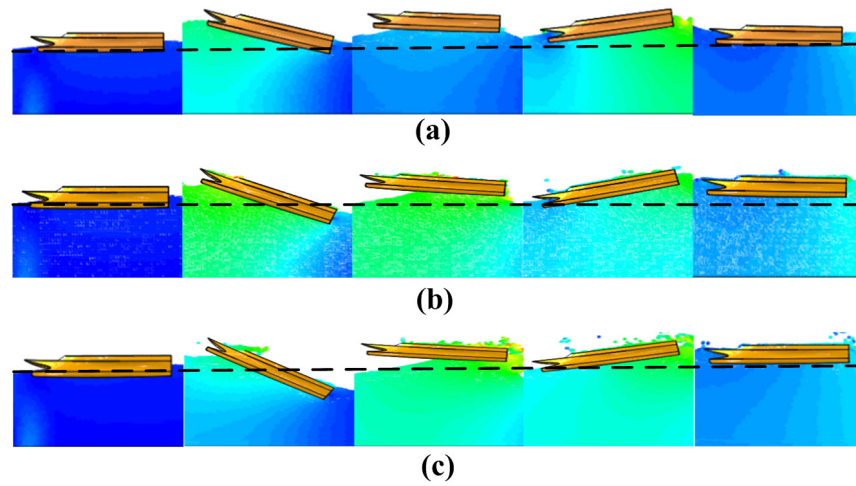


Figure 9. The O&M vessel motion at different speeds. (a) 20 kts. (b) 30 kts. (c) 40 kts.

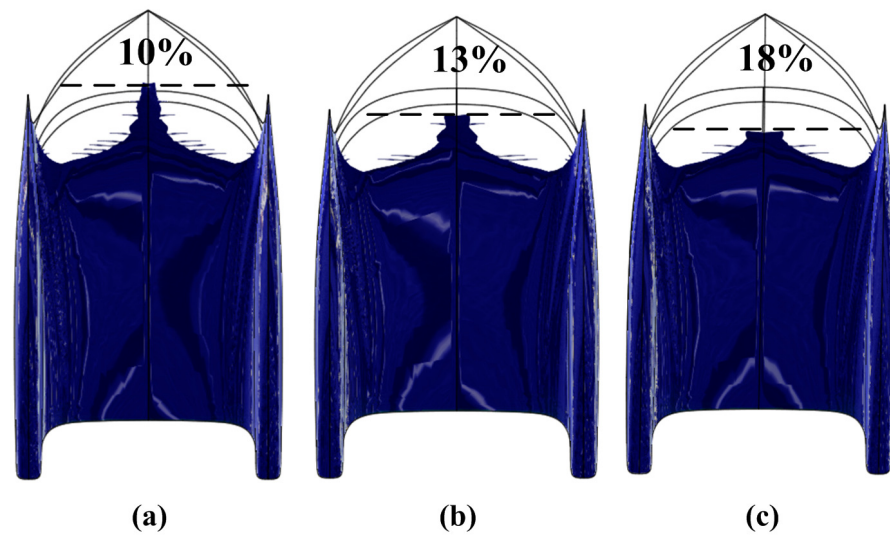


Figure 10. The wetted area of the O&M vessel for different sea states ( $t = 4.6$  s). (a) SSN4. (b) SSN5. (c) SSN6.

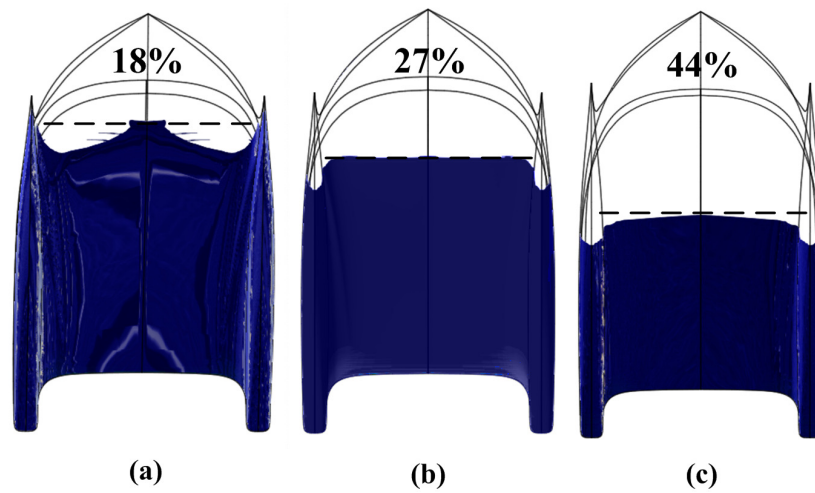


Figure 11. The wetted area of the O&M vessel for different speeds ( $t = 4.6$  s). (a) 20 kts. (b) 30 kts. (c) 40 kts.

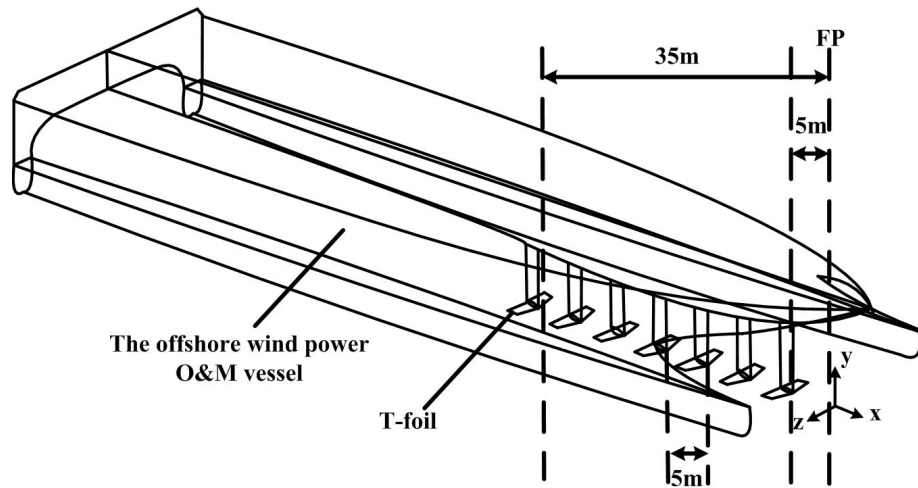


Figure 12. Installation schematic of T-foil.

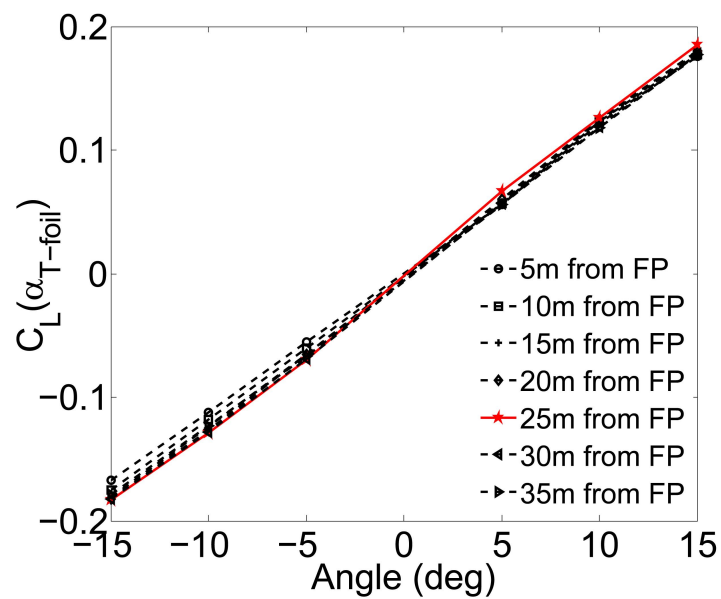


Figure 13. Lift coefficients of T-foil in different installation positions.

Here, the selection of fluid viscosity models needs to be based on the different flow rates in actual situations, which can be divided into laminar flow states with low flow rates and turbulent flow states with high speeds. However, in actual water conditions, the most common fluid flow is often in an unstable and disordered chaotic state with random changes in flow characteristics, namely the turbulent state. The motion equation of turbulence is:

$$\rho \left( \frac{\partial \bar{u}_i}{\partial t} + \bar{u}_j \frac{\partial \bar{u}_i}{\partial j} \right) = \rho m_i - \frac{\partial \bar{p}_i}{\partial i} + \frac{\partial}{\partial j} \left( \mu \frac{\partial \bar{u}_i}{\partial j} - \rho \overline{u'_i u'_j} \right) \quad (i, j = x, y, z) \quad (9)$$

where  $\bar{u}_i$  and  $\bar{u}_j$  are the time-averaged instantaneous velocity of turbulence on the  $x$ ,  $y$ , and  $z$  axes,  $u'_i$  and  $u'_j$  are the mean of the fluctuating velocity of turbulence,  $\bar{p}_i$  is the time average of instantaneous pressure,  $m_i$  is the mass component on the  $x$ ,  $y$ , and  $z$  axes, and  $\mu = \rho \cdot \nu$ ,  $\nu$  is the coefficient of fluid viscosity term.

Figure 13 shows the lift coefficient curves when the different T-foil's attack angles are fixed. It can be seen that when the distance between T-foil and FP is 25 m, the lift coefficient is obviously optimal, and when the distance is beyond this position, the lift coefficient begins to decrease. Therefore, 25 m is the best position to install T-foil for the O&M Vessel.

Depending on the installation of the T-foil's at 25 m, its strut heights can only be made the optional range from 2.55 m–5.15 m. From Figure 14, based on practicability and safety considerations, the biggest strut's height is 5.15 m, and meanwhile the T-foil's main foil is at the same level as the bottom of the demi-hull of the O&M Vessel. The smallest strut's height is 2.55 m, and meanwhile the T-foil's main foil is at the same level as the draft line. Figure 15 shows the lift coefficients of different strut's heights at intervals of 0.65 m. It can be seen that 3.85 m is the optimal option because the lift coefficient of this height is best.

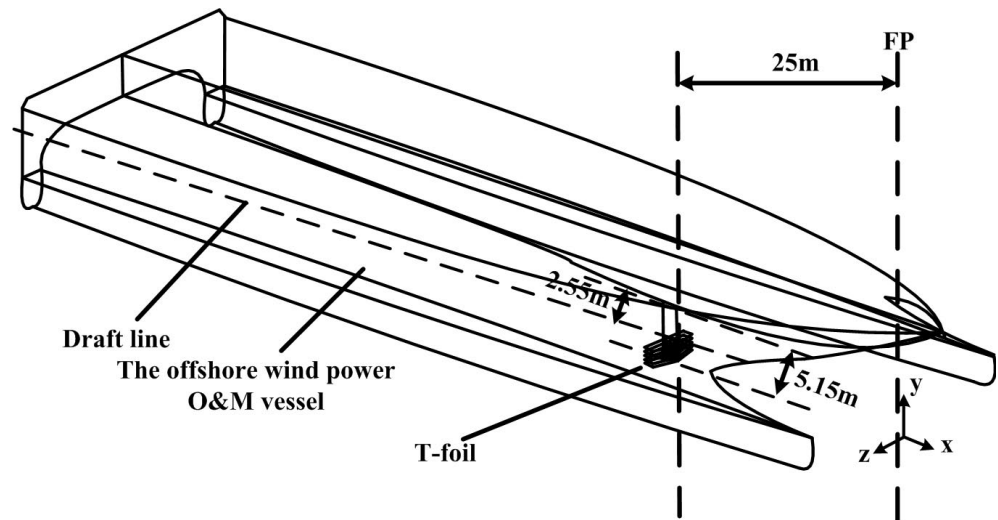


Figure 14. Selections of T-foil's strut height.

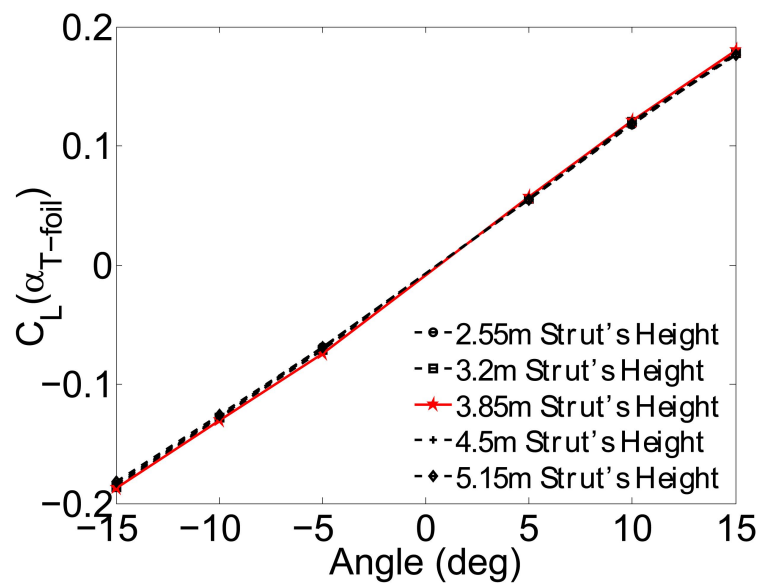


Figure 15. Lift coefficients of T-foil in different strut’s heights.

### 3.3. Characteristics of T-Foil

According to the results of the above optimization analysis, the suitable T-foil model for this O&M vessel is shown in Figure 16 and the parameter details are listed in Table 2 [30].

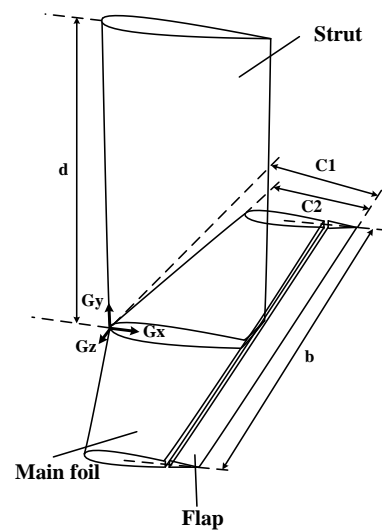


Figure 16. T-foil model.

Table 2. Parameters of T-foil.

Parameters	Sign	Value	Unit
From FP of the O&M vessel	-	25	m
Strut’s height	$d$	3.85	m
Wingspan of main foil	$b$	4.80	m
Chord length of root	C1	1.50	m
Chord length of tip	C2	1.00	m
Aspect ratio	$\frac{b}{c}$	3.84	-
Main foil type	-	NACA0012	-
Strut type	-	NACA16021	-
Rotation angle range	$\alpha_{T-foil}$	-15–15	deg

Figure 17 shows the optimal lift coefficient of the suitable T-foil for the ship. The fitting equation is described as follows:

$$C_L(\alpha_{T-foil}) = p_1\alpha_{T-foil} + p_2 \tag{10}$$

where  $p_1 = 0.01239$ ,  $p_2 = -0.0055$ .

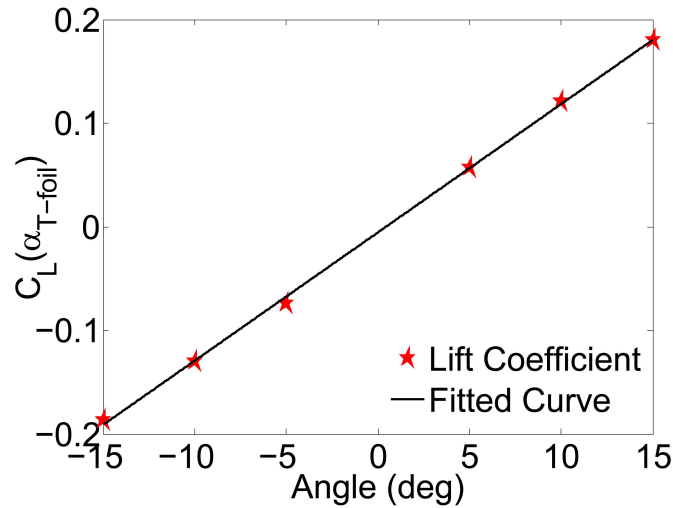


Figure 17. Lift coefficient fitting curve.

#### 4. LQR Controller Design for the O&M Vessel with T-Foil

##### 4.1. Linear Quadratic Regulator Model for the O&M Vessel with T-Foil

Linear quadratic regulator (LQR) [41,42] is a potent technical mean which serves complex systems such as multiple input and multiple output (MIMO) system. The longitudinal control system for the O&M vessel is a MIMO system. In the design of LQR, the optimal control law  $u^*$  can be obtained, and then, the performance index  $J$  is optimized. The performance index  $J$  is defined as follows:

$$J = \frac{1}{2} \int_0^\infty (x^T Q x + u^T R u) dt \tag{11}$$

where  $Q \geq 0$  and  $R > 0$  are quadratic symmetrical matrices. They represent respective weights on state vector  $x$  and control (input) vector  $u$ , which satisfy the linearized anti-heaving and pitching system of this study.

$$\begin{aligned} \dot{x} &= Ax + B_2 u + B_1 d \\ y &= Cx \end{aligned} \tag{12}$$

where  $x = [w, q, z, \theta]^T$  is state variable,  $y = x$  is output variable,  $d$  is wave disturbance signal,  $A$  is the system matrix,  $B_1$  is the wave disturbance matrix,  $B_2$  is the control matrix, and  $C = I_{4 \times 4}$  is the output matrix. The expressions of  $A$ ,  $B_1$ ,  $B_2$  and the variables within each matrix are as follows:

$$\begin{aligned} A &= \begin{bmatrix} -A_a^{-1} B_b & -A_a^{-1} C_c \\ I_{2 \times 2} & 0_{2 \times 2} \end{bmatrix}, B_1 = \begin{bmatrix} A_a^{-1} \\ 0_{2 \times 2} \end{bmatrix} \begin{bmatrix} Z_d \\ M_d \end{bmatrix}, B_2 = \begin{bmatrix} A_a^{-1} \\ 0_{2 \times 2} \end{bmatrix} \begin{bmatrix} Z_u \\ M_u \end{bmatrix}, \\ [A_a] &= \begin{bmatrix} m - Z_{\dot{w}} & Z_{\dot{q}} \\ M_{\dot{w}} & I_{yy} - M_{\dot{q}} \end{bmatrix}, [B_b] = \begin{bmatrix} Z_w & Z_q \\ M_w & M_q \end{bmatrix}, [C_c] = \begin{bmatrix} Z_z & Z_\theta \\ M_z & M_\theta \end{bmatrix}. \end{aligned}$$

Determine the control law  $u^*$  that minimizes the performance index  $J$  under the following LQR design steps.

4.2. Solve the Matrix Algebraic Riccati Equation (ARE)

The Hamilton–Jacobi–Bellman theory is developed in this study to solve the LQR optimal control issue because the performance indicator  $J$  is convex.

Introducing the Hamilton function:

$$H(x, \lambda, u) = \frac{1}{2}(x^T Qx + u^T Ru) + \lambda^T (Ax + B_2u) \tag{13}$$

with the necessary canonical equation and extreme condition:

$$\dot{x} = \frac{\partial H}{\partial \lambda} = Ax + B_2u \tag{14}$$

$$\dot{\lambda} = -\frac{\partial H}{\partial x} = -Qx - A^T \lambda \tag{15}$$

$$\frac{\partial H}{\partial u} = Ru + B_2^T \lambda = 0 \tag{16}$$

From Equation (16), the optimal control  $u^*$  is obtained:

$$u^* = -R^{-1}B_2^T \lambda \tag{17}$$

**Assumption 1.** A linear relationship between  $\lambda$  and  $x$  can be obtained from Equations (14) and (15) that can be written as:

$$\lambda = Px \tag{18}$$

And differentiating between both sides of Equation (18) with respect to the time, we then obtain:

$$\dot{\lambda} = \dot{P}x + P\dot{x} = (\dot{P} + PA - PB_2R^{-1}B_2^T P)x \tag{19}$$

Thus, the preceding Equation (19) becomes as follows by simultaneous Equations (15) and (18).

$$\dot{\lambda} = (\dot{P} + PA - PB_2R^{-1}B_2^T P)x = -Qx - A^T Px \tag{20}$$

**Remark 1.**  $P$  tends to a constant matrix in the infinite time, meanwhile, first derivative of  $P$  tends to zero that is  $\dot{P} \rightarrow 0$ .

Then, according to Equation (20), for any  $x$ , a sufficient condition for optimal control is that the matrix  $P$  must be satisfied:

$$PA + A^T P - PB_2R^{-1}B_2^T P + Q = 0 \tag{21}$$

where  $P$  is the solution of Riccati Equation (21) and it is the symmetric positive definite matrix.

4.3. Obtain the Optimal Control

Combining Equations (17) and (18), the optimal control law  $u^*$  is obtained:

$$u^* = -R^{-1}B_2^T Px^* \tag{22}$$

where  $x^*$  is the optimal state.

**Remark 2.** Letting  $R^{-1}B_2^T P = K$ , and finally the optimal control law  $u^*$  can be rewritten as:

$$u^* = -Kx^* \tag{23}$$

and then, it is found that the optimal control can be determined once  $P$  has been solved.

4.4. Obtain the Minimum Value of Performance Index J

From Equation (24), the minimum value of performance index J can be obtained:

$$J^* = \frac{1}{2}x^{*T}Px^* \tag{24}$$

When the O&M vessel is sailing at 20 kts and SSN6 in head seas, the system matrix A, the wave disturbance matrix B<sub>1</sub>, and the control matrix B<sub>2</sub> are as follows:

$$A = \begin{bmatrix} -1.0673 & -13.8683 & -14.7318 & 8.4357 \\ 0.0322 & -0.8313 & 0.2239 & -15.3339 \\ 1 & 0 & 0 & 0 \\ 0 & 1 & 0 & 0 \end{bmatrix},$$

$$B_1 = \begin{bmatrix} 0.0086 & -2.8 \times 10^{-5} \\ -1.5 \times 10^{-4} & 2.1 \times 10^{-5} \\ 0 & 0 \\ 0 & 0 \end{bmatrix}, B_2 = \begin{bmatrix} 24.8660 \\ 1.6297 \\ 0 \\ 0 \end{bmatrix}.$$

According to the above steps, Q = diag(1, 1, 10, 100) and R = 10 are chosen as the weighting coefficients to trade off the reduction of heave and pitch motion. Therefore, the solution of Riccati equation P and the gain K are as follows:

$$P = \begin{bmatrix} 22.6724 & 1.4870 & 0.4301 & 0.0257 \\ 1.4870 & 0.2513 & 0.0382 & 0.0024 \\ 0.4301 & 0.0382 & 0.8184 & 0.0634 \\ 0.0257 & 0.0024 & 0.0634 & 0.0145 \end{bmatrix}, K = [ 0.2742 \quad 0.7323 \quad 0.5560 \quad 0.6765 ].$$

**Proof of stability analysis.** The LQR controller’s stability analysis is as follows [10]. □

Select the following Lyapunov function:

$$V(x) = x^T Px \tag{25}$$

where for the  $\forall x \neq 0$ , there is a  $V(x) > 0$ , and for the  $\forall \|x\| \rightarrow \infty$ , there is a  $V(x) \rightarrow \infty$ . P remains a symmetric positive definite solution of Equation (21). The first-order time derivative of V(x) is:

$$\dot{V}(x) = \dot{x}^T Px + x^T P\dot{x} \tag{26}$$

Substituting Equations (12), (21) and (23) into Equation (26) yields:

$$\begin{aligned} \dot{V}(x) &= [(A - B_2R^{-1}B_2^T P)x]^T Px + x^T P(A - B_2R^{-1}B_2^T P)x \\ &= x^T (A^T - P^T B_2(R^{-1})^T B_2^T)Px + x^T PAx - x^T PB_2R^{-1}B_2^T Px \\ &= x^T A^T Px - x^T P^T B_2(R^{-1})^T B_2^T Px + x^T PAx - x^T PB_2R^{-1}B_2^T Px \\ &= x^T (A^T P - P^T B_2(R^{-1})^T B_2^T P + PA - PB_2R^{-1}B_2^T P)x \\ &= x^T (-Q - P^T B_2(R^{-1})^T B_2^T P)x \\ &= -x^T (Q + PB_2R^{-1}B_2^T P)x < 0 \end{aligned} \tag{27}$$

The suggested controller stabilizes the system described in Equation (12) using the Lyapunov stability theorem [43].

5. Results and Discussion

5.1. Simulation Results Using LQR Method

Figure 18 shows the anti-heaving and pitching motion system of the O&M vessel. There are two main sections—free O&M vessel block and T-foil active ride control block in the overall block diagram. The section labeled “O&M vessel without T-foil” in dashed frame is a free vessel model, namely that only waves induce the vessel’s heave and pitch

motion. Another labeled “Longitudinal control system of the O&M vessel with T-foil” is a model of the stabilizer which contains the free vessel model and the longitudinal control system composed of stabilizer and proposed controller. The input signal  $u^*$  can be obtained by the aforementioned controller design as the input attack angle of T-foil, and then control forces and moments of T-foil can help to decrease heave and pitch motion.

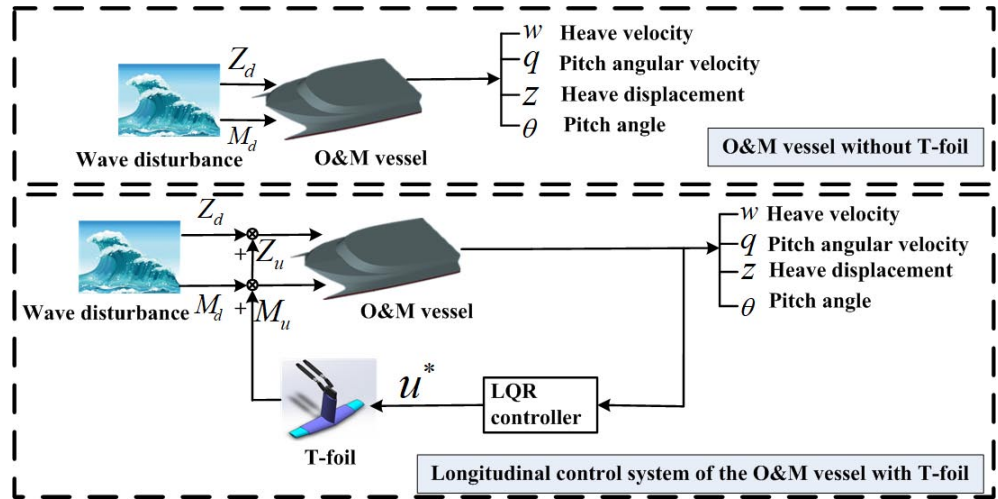


Figure 18. Longitudinal control system of the O&M vessel with T-foil.

The responses of heave and pitch motion are obtained owing to the above building of ride control platform. Taking into account the damage caused by the vessel’s motion to passengers and freight [13], the pitch reduction is preferred in this paper. Figures 19 and 20 show that the T-foil active ride control is feasible and effective at high sailing speed and high sea state for the O&M Vessel. Moreover, as can be shown, pitch reduction outperforms heave. The anti-heaving forces and pitch moments have a better compensation for wave-induced disturbing forces and moments.

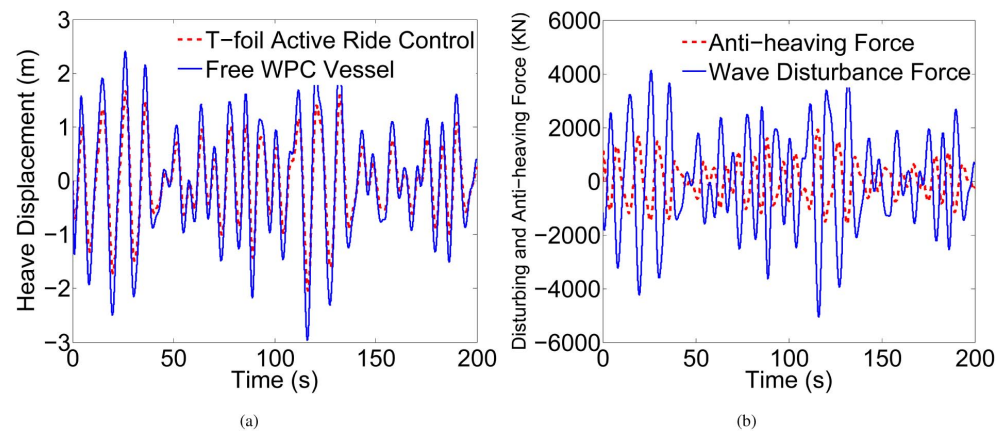
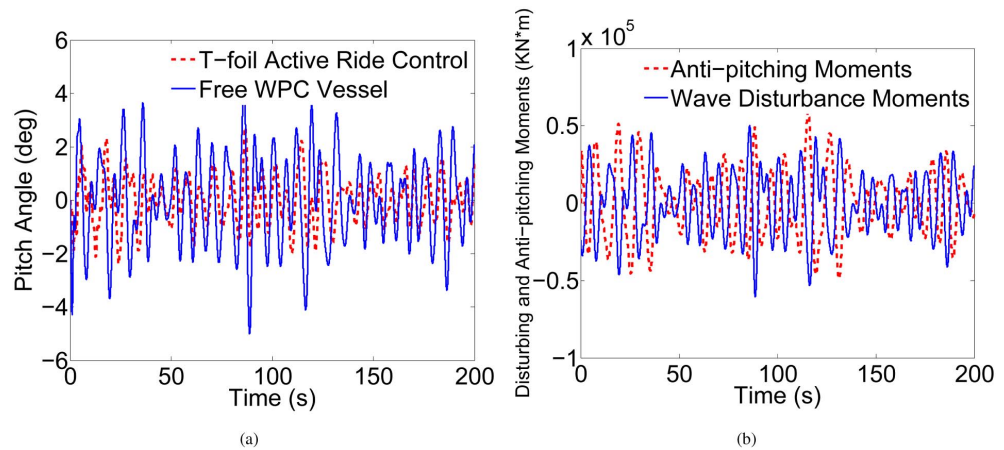


Figure 19. Simulation results of heave at 20 kts and SSN6 in head seas. (a) Heave reduction. (b) Heave disturbing forces and T-foil control forces.



**Figure 20.** Simulation results of pitch at 20 kts and SSN6 in head seas. (a) Pitch reduction. (b) Pitch disturbing moments and T-foil control moments.

5.2. T-Foil Stabilization under Multiple Operating Conditions

The heave and pitch motion responses at different sea states and speeds are shown in Figures 21 and 22. It can be seen that with the increase of sea state, the amplitude of heave and pitch motion increases obviously. However, the increase of the speed does not have much effect on heave and pitch motion. Therefore, we can come to the conclusion that the change of sea state has a greater impact on ship motion compared with the change of speed.

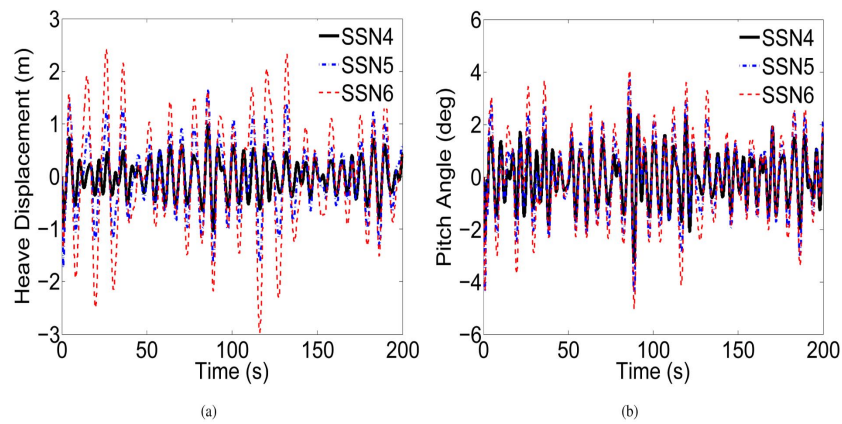


**Figure 21.** Seakeeping performance of the O&M vessel at different sea states. (a) Heave. (b) Pitch.

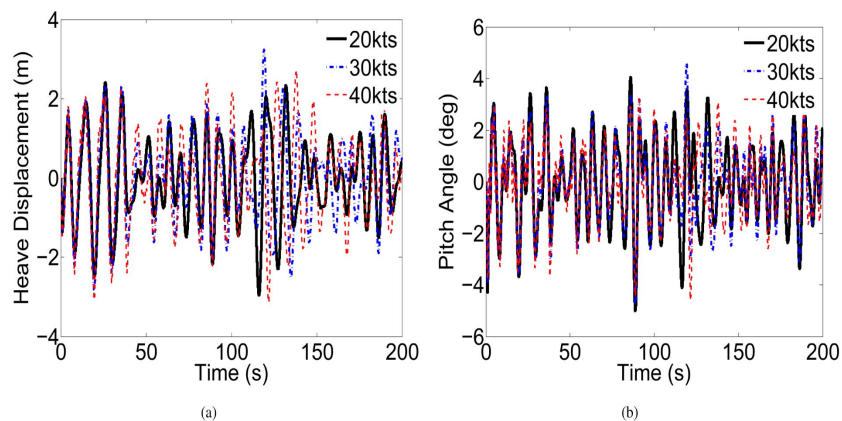


**Figure 22.** Seakeeping performance of the O&M vessel at different speeds. (a) Heave. (b) Pitch.

To investigate the effectiveness of longitudinal control system with T-foil for the O&M vessel, the following evaluation formula was selected to calculate the anti-heaving and pitching effect.

$$E_{PE} = \frac{HPB - HPA}{HPB} \times 100\% \tag{28}$$

where  $E_{PE}$  is anti-heaving and pitching effect,  $HPA$  and  $HPB$  represent the root mean square (RMS) of the heave displacement and pitch angle with and without the T-foil active longitudinal control system, respectively [44].

This paper pays attention to the situations of high sea states and speeds for the offshore wind power O&M vessel. The simulation results of the anti-heaving and pitching effect at the considered same speed 20 kts and different high sea states (SSN4, SSN5, and SSN6), and the same sea state SSN6 and different high sailing speeds (20 kts, 30 kts, and 40 kts) with encounter angle  $180^\circ$  are depicted in Figure 23. As is shown in Figure 23, the anti-heaving effect of T-foil active longitudinal control system is above 20% and most of them are above 30% at different sea states and speeds. This result satisfies the reduction index of the O&M vessel. However, the anti-heaving effect at 40 kts and SSN6 just reaches 20.18% because of the worst sea environment in this paper. This further illustrates that it is difficult to control the attitude of ship at high sea states and speeds. In addition, the anti-pitching effect is above 40% at different sea states and speeds. There is 10% points higher than that of heave, which confirms the description of Figures 19 and 20. It can be concluded that the T-foil active longitudinal control system with the proposed controller is promising and effective for the heave and pitch reduction of the O&M vessel.

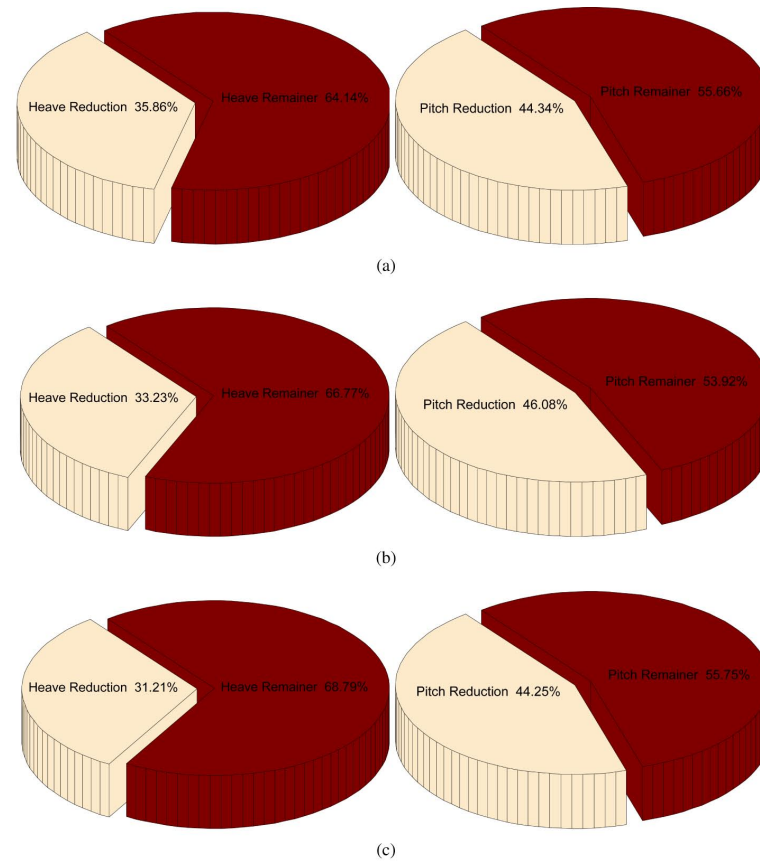
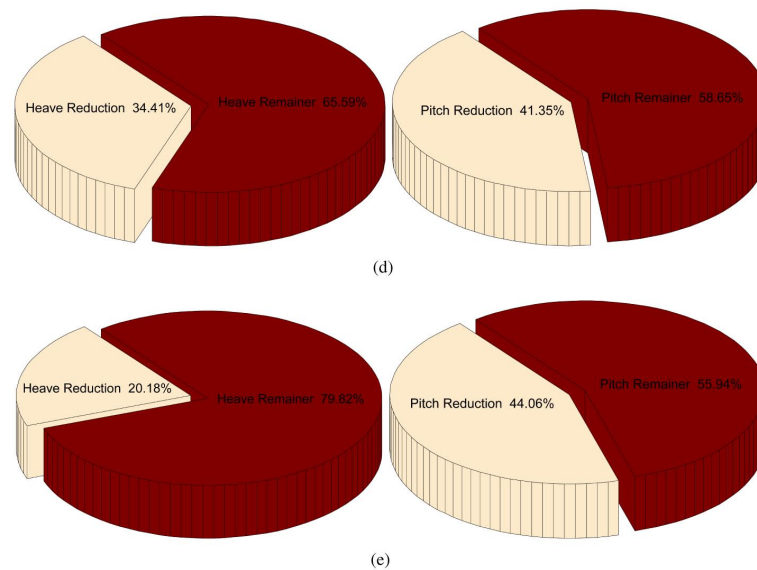


Figure 23. Cont.



**Figure 23.** Heave and pitch reductions for the O&M vessel in different situations. (a) Reduction for SSN4, 20 kts. (b) Reduction for SSN5, 20 kts. (c) Reduction for SSN6, 20 kts. (d) Reduction for SSN6, 30 kts. (e) Reduction for SSN6, 40 kts.

## 6. Conclusions

A suitable stabilizer is the core of the ride control system for a ship. In this paper, a reduced scale ship simulation model was used to find the range of the installation of T-foil preliminarily. Following that, through the CFD simulation of different positions, the optimum T-foil's installation was determined. Next, the optimal strut's height of T-foil can be obtained by CFD software in different height situations after the determination of the position. Therefore, the most suitable T-foil was obtained for a certain catamaran. In addition, this paper introduces a 2 DOF motion model with detailed disturbing and control forces and moments. Based on the ship motion model, a longitudinal control system with LQR controller was established, including free vessel block and the suitable T-foil active ride control block. In conclusion, the simulation results of heave and pitch reduction indicate that the longitudinal control system-based suitable T-foil stabilizer and stated controller is both practicable and efficient to ensure the O&M vessel motion reduction.

Future work will be focused on extension of the present models (e.g., 4 DOF model and 6 DOF model) and will add a motion sickness incidence model to measure passenger comfort in the final evaluation method. The implementation of real ship model experiments can further improve the motion model and controller design methods.

**Author Contributions:** Conceptualization, J.Y. and L.L.; methodology, J.Y. and S.Z.; software, J.Y. and P.Z.; validation, Z.L.; formal analysis, Z.L.; investigation, J.Y. and Z.L.; resources, J.Y.; data curation, H.G., S.Z. and P.Z.; writing—original draft preparation, J.Y.; writing—review and editing, Z.L.; visualization, J.Y.; supervision, Z.L., H.G. and L.L.; project administration, J.Y.; funding acquisition, J.Y., Z.L. and H.G. All authors have read and agreed to the published version of the manuscript.

**Funding:** This research was funded by Science and Technology Project of Hebei Education Department grant number QN2021034, the Natural Science Foundation of Hebei Province of China grant number F2019402419 and the Innovation Fund Project of Hebei University of Engineering grant number SJ230100695, SJ220100317.

**Institutional Review Board Statement:** Not applicable.

**Informed Consent Statement:** Not applicable.

**Data Availability Statement:** The authors confirm that the data supporting the findings of this study are available within the article.

**Conflicts of Interest:** The authors declare no conflict of interest.

## Abbreviations

The following abbreviations are used in this manuscript:

O&M	Operation and maintenance
4 DOF	Four degrees of freedom
MSI	Motion sickness incidence
RCS	Ride control system
LQG	Linear quadratic Gaussian
2 DOF	Two degrees of freedom
CFD	Computer fluid dynamic
SSN	Sea state numbers
M DOF	Multiple degrees of freedom
6 DOF	Six degrees of freedom
LQR	Linear quadratic regulator
CG	Center of gravity
PSD	Power spectral density
PM	Pierson-Moskowitz
FP	Forward perpendicular
MIMO	Multiple input and multiple output
ARE	Algebraic riccati equation
RMS	Root mean square

## References

- Zhang, S.; Zhao, P.; Li, C.; Song, Z.; Liang, L. Study on the Accessibility Impact of Anti-Rolling Tank on the Offshore Wind O&M Gangway. *J. Mar. Sci. Eng.* **2023**, *11*, 848.
- Fan, Q.; Wang, X.; Yuan, J.; Liu, X.; Hu, H.; Lin, P. A Review of the Development of Key Technologies for Offshore Wind Power in China. *J. Mar. Sci. Eng.* **2022**, *10*, 929. [[CrossRef](#)]
- Liang, L.; Cheng, Q.; Li, J.; Le, Z.; Cai, P.; Jiang, Y. Design of the roll and heel reduction controller on ship's turning motion. *Ocean Eng.* **2023**, *284*, 115093. [[CrossRef](#)]
- Jin, Z.; Liu, S.; Jin, L.; Chen, W.; Yang, W. Model based robust predictive control of ship roll/yaw motions with input constraints. *Appl. Sci.* **2020**, *10*, 3377. [[CrossRef](#)]
- Ren, R.; Zou, Z.; Wang, J. Time-scale decomposition techniques used in the ship path-following problem with rudder roll stabilization control. *J. Mar. Sci. Eng.* **2021**, *9*, 1024. [[CrossRef](#)]
- Lee, S.; Hwang, S.; Kim, H.; Hyun, Y.; Lee, S.; Paik, K. A numerical study on the hydrodynamic performance of a tanker in bow sea conditions depending on restraint conditions. *J. Mar. Sci. Eng.* **2023**, *11*, 1726. [[CrossRef](#)]
- Li, M.; Shan, L.; Xu, G.; Xu, W.; Wang, J. Experimental and numerical study of the hydrodynamics of a flapping fin at zero speed. *Ocean Eng.* **2023**, *288*, 115945. [[CrossRef](#)]
- Song, J.; Zhao, P.; Liang, L.; Ji, M. Force modeling of zero/low-velocity fin stabilizer and hydrofoil profile optimization. *Ocean Eng.* **2020**, *213*, 107635. [[CrossRef](#)]
- Deniz, O. Performance of a Magnus effect-based cylindrical roll stabilizer on a full-scale Motor-yacht. *Ocean Eng.* **2020**, *218*, 108247.
- Liang, L.; Jiang, Y.; Zhang, Q.; Le, Z. Aspect ratio effects on hydrodynamic characteristics of Magnus stabilizers. *Ocean Eng.* **2020**, *216*, 107699. [[CrossRef](#)]
- Liang, L.; Yuan, J.; Zhang, S.; Zhao, P. Design a software real-time operation platform for wave piercing catamarans motion control using linear quadratic regulator based genetic algorithm. *PLoS ONE* **2018**, *13*, e0196107. [[CrossRef](#)] [[PubMed](#)]
- Li, J.; Li, Z.; Wu, Y.; Xiong, X.; Li, Z.; Xiong, W. Research on high-speed catamaran motion reduction with semi-active control of flexible pontoon. *J. Mar. Sci. Eng.* **2023**, *11*, 1747. [[CrossRef](#)]
- Esteban, S.; Giron-Sierra, J.; Andres-Toro, D.; Cruz, J.; Riola, J. Fast ships models for seakeeping improvement studies using flaps and T-Foil. *Math. Comput. Model.* **2005**, *41*, 1–24. [[CrossRef](#)]
- Zong, Z.; Sun, Y.; Jiang, Y. Experimental study of controlled T-foil for vertical acceleration reduction of a trimaran. *J. Mar. Sci. Technol.* **2019**, *24*, 553–564. [[CrossRef](#)]
- Zhu, Q.; Ma, Y. A design of T-foil and trim tab for fast catamaran based on NSGA-II. *J. Hydrodyn.* **2020**, *32*, 161–174. [[CrossRef](#)]
- Zhu, Q.; Ma, Y. Design of  $H_{\infty}$  anti-vertical controller and optimal allocation rule for catamaran T-foil and trim tab. *J. Ocean Eng. Mar. Energy* **2019**, *5*, 205–216. [[CrossRef](#)]
- Ma, Y.; Zhu, Q. Fast trimaran anti-longitudinal motion control system based on active disturbance rejection control with controller tuning. *J. Mar. Sci. Technol.* **2022**, *27*, 1045–1064. [[CrossRef](#)]
- Lau, C.; Ali-Lavroff, J.; Holloway, D.; Shabani, B.A.; Mehr, J.; Thomas, J. Influence of an active T-foil on motions and passenger comfort of a large high-speed wave-piercing catamaran based on sea trials. *J. Mar. Sci. Technol.* **2022**, *27*, 856–872. [[CrossRef](#)]
- Jiang, Y.; Bai, J.; Liu, S.; Zong, Z.; Li, P. Experimental investigation of T-foil hybrid control strategy for ship motion reduction in head seas. *Ocean Eng.* **2022**, *243*, 110251. [[CrossRef](#)]

20. Esteban, S. Modelado y Control del Movimiento Longitudinal de un Ferry de Alta Velocidad. Ph.D. Thesis, Universidad Complutense de Madrid, Madrid, Spain, 2002.
21. Liang, L.; Yuan, J.; Zhang, S.; Liu, Y. Simulation study on wave piercing catamarans based on T-foil optimization model. *J. Huazhong Univ. Sci. Tech.* **2018**, *46*, 7–12.
22. Davis, M.; Watson, N.; Holloway, D. Wave response of an 86m high speed catamaran with active T-foils and stern tabs. *Int. J. Marit. Eng.* **2003**, *145*, 15–34.
23. Shen, Y.; Chen, M.; Skelton, R. Markov data-based reference tracking control to tensegrity morphing airfoils. *Eng. Struct.* **2023**, *291*, 116430. [[CrossRef](#)]
24. Chota, T.;Takanori, H.; Youhei, T. Numerical analysis of wake wash reduction for catamaran with hydrofoils. *Appl. Ocean Res.* **2023**, *135*, 103556.
25. Liu, Z.; Zheng, L.; Li, G.; Yuan, S.; Yang, S. An experimental study of the vertical stabilization control of a trimaran using an actively controlled T-foil and flap. *Ocean Eng.* **2021**, *219*, 108224. [[CrossRef](#)]
26. Liang, C.; Zhang, X. Concise and economical control implemented on ship fin stabilizer system based on nonlinear feedback algorithm. *J. Mar. Sci. Technol.* **2021**, *26*, 88–96. [[CrossRef](#)]
27. Chang, W.; Chang, C.; Lin, Y.; Du, J. Discrete-time robust fuzzy control synthesis for discretized and perturbed ship fin stabilizing systems subject to variance and pole location constraints. *J. Mar. Sci. Technol.* **2021**, *26*, 201–215. [[CrossRef](#)]
28. Zhang, J.; Liu, Z.; Sun, T.; Bu, M. Explicit stochastic model predictive control for anti-pitching a high-speed multihull. *Appl. Ocean Res.* **2022**, *119*, 102917. [[CrossRef](#)]
29. Cao, T.; Zhang, X. Nonlinear Decoration Control Based on Perturbation of Ship Longitudinal Motion Model. *Appl. Ocean Res.* **2023**, *130*, 103412. [[CrossRef](#)]
30. Sicard, B. Non-Magnetic Pitch and Heave Stabilizing T-Foil. Master's Thesis, Royal Institute of Technology University, Stockholm, Sweden, 2002.
31. Fossen, T. *Guidance and Control of Ocean Vehicles*; John Wiley and Sons: Hoboken, NJ, USA, 1994.
32. Chin, C.; Lin, W.; Lin, J. Experimental validation of open-frame ROV model for virtual reality simulation and control. *J. Mar. Sci. Technol.* **2018**, *23*, 267–287. [[CrossRef](#)]
33. Prestero, T. *Verification of a Six-Degree of Freedom Simulation Model for the REMUS Autonomous Underwater Vehicle*; MIT Press: Cambridge, MA, USA, 2001.
34. Tiwari, B.; Sharma, R. Design and analysis of a variable buoyancy system for efficient hovering control of underwater vehicles with state feedback controller. *J. Mar. Sci. Eng.* **2020**, *8*, 263. [[CrossRef](#)]
35. Dai, Y.; Liu, L.; Feng, S. On the identification of coupled pitch and heave motions using opposition-based particle swarm optimization. *Math. Probl. Eng.* **2014**, *2014*, 784049. [[CrossRef](#)]
36. Perez, T.; Blanke, M. *Simulation of Ship Motion in Seaway*; Technical Report; The University of Newcastle: Callaghan, Australia, 2005.
37. Price, W.; Bishop, R. *Probabilistic Theory of Ship Dynamics*; Chapman and Hall: London, UK, 1974.
38. Wang, Z.; Yuan, T.; Kong, X.; Wu, W. A universal similarity method and design procedure for buckling assessment of stiffened plates under compression load on real ships. *Thin-Walled Struct.* **2022**, *181*, 110025. [[CrossRef](#)]
39. Khomyakov, A.; Elyukhina, I. Complete dynamic similarity for sea trials and towing tank experiments by means of polymer drag reduction. *Ocean Eng.* **2019**, *178*, 31–37. [[CrossRef](#)]
40. Sclavounos, P.; Borgen, H. Seakeeping analysis of a high speed monohull with a motion control bow hydrofoil. *J. Ship Res.* **2004**, *48*, 77–117. [[CrossRef](#)]
41. Lv, Y.; Li, H. Strong fixed-time dynamic inverse adaptive LQR integrated control strategy for dynamic positioning of ship. *Ocean Eng.* **2023**, *288*, 115969. [[CrossRef](#)]
42. Moradi, M.; Bayat, F.; Charmi, M. A salient object detection framework using linear quadratic regulator controller. *J. Vis. Commun. Image Represent.* **2021**, *79*, 103259. [[CrossRef](#)]
43. Merabet, A. Adaptive sliding mode speed control for wind energy experimental system. *Energies* **2018**, *11*, 2238. [[CrossRef](#)]
44. Yuan, J. Research on Ride Control System for Wave Piercing Catamarans Based T-Foil and Stern Flaps. Ph.D. Thesis, Harbin Engineering University, Harbin, China, 2019.

**Disclaimer/Publisher's Note:** The statements, opinions and data contained in all publications are solely those of the individual author(s) and contributor(s) and not of MDPI and/or the editor(s). MDPI and/or the editor(s) disclaim responsibility for any injury to people or property resulting from any ideas, methods, instructions or products referred to in the content.